Video Article

Atomically Traceable Nanostructure Fabrication

Josh B. Ballard[1], Don D. Dick[2], Stephen J. McDonnell[3], Maia Bischof[4], Joseph Fu[5], James H. G. Owen[1], William R. Owen[1], Justin D. Alexander[1], David L. Jaeger[4], Pradeep Namboodiri[5], Ehud Fuchs[1], Yves J. Chabal[3], Robert M. Wallace[3], Richard Reidy[4], Richard M. Silver[5], John N. Randall[1], James Von Ehr[1]

[1]Zyvex Labs

[2]Department of Physics, University of Texas at Dallas

[3]Department of Materials Science and Engineering, University of Texas at Dallas

[4]Materials Science and Engineering, University of North Texas

[5]National Institute of Standards and Technology

Correspondence to: Josh B. Ballard at jballard@zyvexlabs.com

URL: http://www.jove.com/video/52900
DOI: doi:10.3791/52900

Keywords: Engineering, Issue 101, Nanolithography, Scanning Tunneling Microscopy, Atomic Layer Deposition, Reactive Ion Etching

Date Published: 7/17/2015

Citation: Ballard, J.B., Dick, D.D., McDonnell, S.J., Bischof, M., Fu, J., Owen, J.H.G., Owen, W.R., Alexander, J.D., Jaeger, D.L., Namboodiri, P., Fuchs, E., Chabal, Y.J., Wallace, R.M., Reidy, R., Silver, R.M., Randall, J.N., Von Ehr, J. Atomically Traceable Nanostructure Fabrication. *J. Vis. Exp.* (101), e52900, doi:10.3791/52900 (2015).

Abstract

Reducing the scale of etched nanostructures below the 10 nm range eventually will require an atomic scale understanding of the entire fabrication process being used in order to maintain exquisite control over both feature size and feature density. Here, we demonstrate a method for tracking atomically resolved and controlled structures from initial template definition through final nanostructure metrology, opening up a pathway for top-down atomic control over nanofabrication. Hydrogen depassivation lithography is the first step of the nanoscale fabrication process followed by selective atomic layer deposition of up to 2.8 nm of titania to make a nanoscale etch mask. Contrast with the background is shown, indicating different mechanisms for growth on the desired patterns and on the H passivated background. The patterns are then transferred into the bulk using reactive ion etching to form 20 nm tall nanostructures with linewidths down to ~6 nm. To illustrate the limitations of this process, arrays of holes and lines are fabricated. The various nanofabrication process steps are performed at disparate locations, so process integration is discussed. Related issues are discussed including using fiducial marks for finding nanostructures on a macroscopic sample and protecting the chemically reactive patterned Si(100)-H surface against degradation due to atmospheric exposure.

Video Link

The video component of this article can be found at http://www.jove.com/video/52900/

Introduction

As nanotechnology becomes more important in a wide variety of arenas, understanding the structures being formed gains importance, especially in fields of lithography and electronics. To emphasize the importance of metrology at the nanoscale, specifically at scales below 10 nm, it should be pointed out that a variation in feature size of only 1 nm indicates a fractional variation at least 10%. This variation can have significant implications for device performance and material character.[1,2–4] Using synthetic methods, very precisely formed individual features such as quantum dots or other complex molecules can be fabricated,[2,5,6] but generally lacking the same precision in feature placement and orientation, despite work toward improving size and placement control. This paper demonstrates an approach for fabricating nanostructures with near atomic size precision and atomic precision in feature placement, as well as with atomic metrology in feature placement. Using the atomic precision of Scanning Tunneling Microscope (STM) induced Hydrogen Depassivation Lithography (HDL), atomically precise patterns with chemically sensitive contrast are formed on a surface. Selective Atomic Layer Deposition (ALD) then applies a hard oxide material in the patterned areas, with Reactive Ion Etching (RIE) ultimately transferring the patterns into the bulk material, as shown schematically in **Figure 1**. Combining the highly precise HDL process with the standard ALD and RIE processes results in a flexible method to produce nanostructures on a surface with arbitrary shape and positioning.

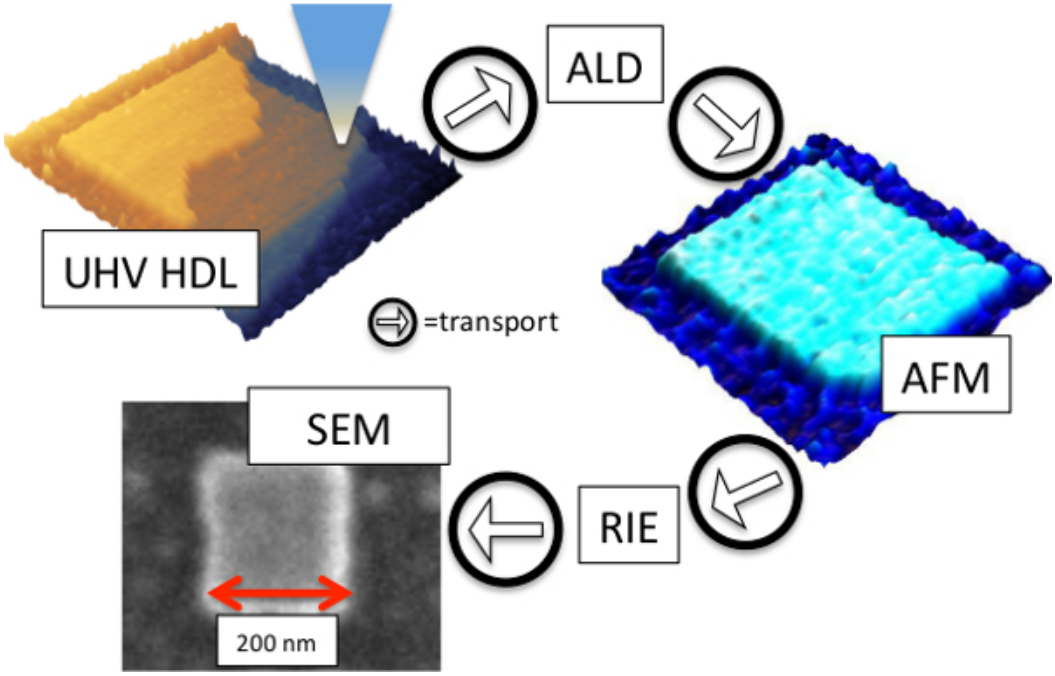

Figure 1. Primary Nanofabrication Process Steps. As an example, a 200 nm x 200 nm square is shown. Each circled arrow indicates a step of atmospheric exposure and transport between sites. After UHV sample prep, the sample is patterned using UHV HDL followed by STM metrology (top left). ALD is then performed, followed by AFM metrology (right). RIE transfers the patterns into Si(100), followed by SEM metrology (bottom left). Please click here to view a larger version of this figure.

The most precise lithography to date usually involves scanned probe techniques, specifically STM-based patterning where atomic resolution patterning and functionalization has been demonstrated for many applications.[7] Previously, atom manipulation has produced nanostructures with ultimate precision by using individual atoms as building blocks,[8,9,10] but the nanostructures required cryogenic conditions and thus lacked long-term robustness. RT atom manipulation by removal of hydrogen atoms from the surface has been shown, specifically HDL.[11,12,13] HDL promises to enable new classes of electronic and other devices based on the spatial localization of surface contrast. Using HDL without further processing, various device architectures are possible including dangling bond wires or logic devices.[14,15,16] In addition to providing electrical contrast, HDL can introduce chemical contrast on the surface where the passivating H layer has been removed, in effect creating a template for further chemical modification. This chemical modification has been demonstrated on silicon and other surfaces, showing selectivity for deposition of metals,[17] insulators,[18] and even semiconductors.[16,19] Each of these examples produces two dimensional structures, so other processing steps must be used to produce true three dimensional structures with the atomically resolved control promised by HDL. Previously, this has required repeated patterning,[19,20,21] annealing,[22] or less well resolved processes such as tip-based e-beam induced deposition.[23]

Similar to e-beam lithography, HDL uses a localized flux of electrons to expose a resist. Several similarities exist such as the capacity to perform multi-mode lithography with variable spot size and patterning efficiency.[24] However, the true power of HDL arises from how it differs from e-beam lithography. First, the resist in HDL is a monolayer of atomic hydrogen so that resist exposure becomes a digital process; the resist atom either is or is not present.[25] Since the H atom placement corresponds to the underlying Si(100) lattice the HDL process can be an atomically precise process, although it should be noted that in this paper the HDL has nanometer precision as opposed to having atomic perfection and thus is not digital in this case. Since the electron source in HDL is local to the surface, the various modes of STM operation facilitate both throughput optimization as well as error checking. At tip-sample biases below ~4.5 V, lithography may be performed at the single atom level with atomic precision, known as Atomically Precise mode (AP mode). In contrast, at biases above ~7 V, electrons are emitted directly from the tip to the sample with wide linewidths and high depassivation efficiencies, known here as Field Emission mode (FE mode). HDL throughputs can then be optimized by careful combination of these two modes, although the overall throughputs remain small relative to e-beam lithography with patterning up to 1 μm^2/minute possible. When the bias is reversed so that the sample is held at ~-2.25 V, electrons tunnel from the sample to the tip with extremely low depassivation efficiency, thus permitting inspection of the atomic structure of the surface both for error correction and for atomic scale metrology.

This nanostructure fabrication process shown in **Figure 1** starts with an UHV-HDL step, as described above. Following HDL, the sample is vented to atmosphere, at which time the patterned areas become saturated with water, forming a thin (*i.e.*, ~1 monolayer) SiO_2 layer.[26] After transport, the sample is inserted into an ALD chamber for deposition of titania (TiO_2), with thicknesses around 2-3 nm deposited here, as measured by AFM and XPS.[27] Since the titania reaction depends upon a water saturation of the surface, this process is possible despite atmosphere exposure which saturates the surface with water. Next, to transfer the ALD mask pattern into the bulk the sample was etched using RIE so that 20 nm of Si is removed, with the etch depth determined by AFM and SEM. In order to facilitate metrology steps, an Si(100) wafer is patterned with a grid of lines which are designed to be visible after UHV preparation by a long working distance optical microscope, AFM plan-view optical imaging, and low-magnification plan-view SEM imaging. To help identify the nanoscale structures, 1 μm^2 serpentine patterns (*serps*) are patterned onto the samples with the most isolated nanopatterns located at fixed locations relative to the *serps*.

This combination of HDL, selective ALD, and RIE can be an important process for nanostructure fabrication, and it includes an atomic scale metrology as a natural byproduct of the process. Below, we include a detailed description of the steps involved to fabricate sub-10 nm nanostructures in Si(100) using HDL, selective ALD, and RIE. It is assumed that one is skilled in each of these processes, but information will be

included related to how to integrate the various processes. Particular emphasis will be given to those unexpected difficulties experienced by the authors in order to prevent the same difficulties, especially related to transport and metrology.

Protocol

1. *Ex-Situ* Sample Preparation

1. Prepare chips
    1. Design appropriate etch mask to put identifying markers in the Si(100) wafer. Using standard optical lithography and RIE, etch a grid of lines as fiducial marks into the wafer from which STM samples will be taken. The lines should be 10 µm wide, 1 µm deep, and at pitch of 500 µm. After etching, strip remaining photoresist from sample.
    Note: The fiducial marks must be identifiable *in-situ* for tip location on the sample as well as in AFM and SEM during metrology.
    2. Protect wafer surface by applying standard tack blue dicing tape, tacky side down.
    3. Dice wafers into chips using a diamond tipped ceramic dicing saw into sizes appropriate for the specific UHV-STM tool being used to perform HDL. Here, the samples were 8.1 mm x 8.1 mm squares.

2. After dicing, prepare chip for insertion into UHV-STM patterning tool by gently peeling back the dicing tape, taking care not to touch chip with any nickel-containing tools which will induce an unfavorable surface reconstruction after UHV prep in section 2 below.
    1. Clean chip by rinsing the front face for 10 sec each with streams of acetone, isopropyl alcohol, methanol, and deionized water, respectively, while gripping the sides of the sample with polytetrafluoroethylene (PTFE) tweezers. Finally, dry with ultrapure N_2 or Ar, still gripping with Teflon tweezers.
    2. Mount sample chip in STM sample holder using methods appropriate for the specific UHV-STM tool to be used for HDL.
        1. If mounting in a nickel-containing sample holder, cut tantalum foil barrier strips (appx. 4 mm by sample height) using titanium scissors. Sonicate foil strips for 5 min each in ultrapure acetone, isopropyl alcohol, methanol, and DI water, respectively. Dry with ultrapure N_2 gas by partially covering a beaker with aluminum foil and injecting an N_2 nozzle into the opening. Flow gas until all liquid has evaporated. Using nickel free tweezers, form foil around ends of sample then clamp in sample holder to isolate front and back sides of sample from sample holder.

    3. After mounting, plasma clean sample and sample holder in oxygen plasma to remove carbon contamination.[28]

2. UHV Sample Preparation

1. Introduce sample into UHV system via load-lock or another preferred UHV-safe method so that the UHV processing and HDL can typically remain below 1.3 x 10^{-9} mbar (except for step 2.5.1.1 below).
2. Degas O/N at 650 °C, monitoring the temperature with a pyrometer. Ensure that the chamber pressure is within 25% of background. In the case described here, typical background pressures are approximately 4.5 x 10^{-10} mbar.
3. Degas tungsten hydrogen cracking filament at 1,500 °C for 5 min. Activate titanium sublimation pumps if possible.
4. Perform sample “Flash” cycle.
    1. Flash sample by heating to 1,250 °C for 20 sec, monitoring T with pyrometer and using a 10 °C/sec heating gradient. Do not exceed a maximum pressure of 7 x 10^{-9} mbar. Cool by removing heating current in less than 5 sec.
    2. Rest sample at 350 °C for 5 min. to allow pressure to recover to baseline. Repeat 3x.

5. Perform sample passivation.
    1. Set sample temperature to 350 °C using a pyrometer to monitor the temperature. Introduce 1.3 x 10^{-6} mbar ultra-pure H_2 into prep chamber using leak valve.
        1. Put a cold trap on the H_2 line very near a leak valve in the system in order to further purify H_2.
        2. If possible, pump system with high-velocity turbo pump instead of an ion pump. This is so the ion pump does not contaminate the sample from being exposed to the high pressured and ejecting contaminants. The pumps are put back in the normal state after most the hydrogen has been removed and the sample is still warm (350 °C).

    2. Turn on tungsten hydrogen cracking filament to a temperature of 1,400 °C for 12 min, then turn off filament and H_2 gas flow. Cool sample to RT.

3. Scanning Tunneling Microscopy and Lithography

1. Transfer sample to STM, and bring sample and STM tip into tunneling range. Using a camera with resolving power of better than a 20 µm spot size, take high-resolution optical image of tip-sample junction. Deskew and resize the optical image so that it represents an undistorted reproduction of the fiducial marks.
2. Remove any illumination to reduce system thermal instabilities. Determine surface quality.
    1. Using conventional STM techniques with sample bias of -2.25 V and 200 pA, identify the number of defects on the surface.
    2. If surface defects are below acceptable levels, move to the next step. Maximum acceptable defect levels are as followed: Dangling bonds of 1%; Si vacancies of 3%; contaminants of 1%.

3. Design HDL patterns to be produced, including both experimental patterns and large (1 µm x 1 µm) *serp* identification patterns. The *serp* patterns should be drawn with a long vector axis perpendicular to expected AFM fast scan axis, using a pitch of 15-20 nm. Fracture overall pattern into fundamental shapes to define the path followed by the tip when applying HDL conditions.[24]

4. Using vector outputs from the previous step, perform HDL using FE mode lithography for large areas with sample bias of 7-9 V, current of 1 nA, and 0.2 mC/cm and AP mode lithography for small areas or those areas requiring atomic precision edges.[24]
    1. Determine optimal AP mode lithography conditions by performing HDL with an variety of conditions with sample bias ranging from 3.5 to 4.5 V, current ranging from 2 to 4 nA, and line dosages ranging from 2 to 4 mC/cm. Choose conditions that produce the narrowest completely depassivated line.

5. Perform STM metrology on desired HDL patterned areas by imaging at -2.25 V sample bias and 0.2 nA tunneling current.
    1. [optional] Perform error correction. After STM metrology, compare depassivation pattern in the STM images with the desired pattern from step 3.5. If any areas show insufficient dangling bond formation, repeat the lithography cycle in those areas.

6. After completing STM HDL, disengage tip from sample, and move sample to load lock.
7. Vent and remove sample. During vent with ultrapure N_2, protect sample by contacting it with inert, flat substrate such as clean sapphire.[29] After surface protection, close valves to any pumps then introduce vent gas as quickly as possible. Remove sample from system.

4. Sample Transport

1. Remove sample from load lock. Release sample from sample holder, including removing the foil barrier pieces if possible. Using PTFE (or Ti) tweezers, move sample to transporter, keeping front side of sample protected, attempting to keep atmosphere exposure to less than 10 min.
2. Install cover over sample and loosely assemble a pressurized sample transporter. Flush with ultrapure Ar for 1 min. ***Do not evacuate system at any point, or surface damage may occur.***[29] Finally, seal sample transporter with a small positive pressure (~50-100 mbar) of Ar so that the sample remains stable for up to a month.

5. Atomic Layer Deposition

1. Ensure the ALD is at the proper deposition temperature (100 °C). Slowly increase the argon pressure in the ALD chamber until atmospheric pressure has been achieved.
2. Open ALD chamber.
3. Open sample transporter and quickly transfer to ALD chamber using a pair of PTFE tweezers grasping the sample on edge, then close the ALD chamber and purge using a flow of argon at a pressure of $< 2 \times 10^{-1}$ mbar for 1 hr to degas the sample. Set a process to perform 80 repeated cycles of ALD to grow 2.8 nm of amorphous titania.
    1. Using an unmodified commercial ALD system at a sample temperature of 100-150 °C, with titanium tetrachloride ($TiCl_4$) and water (H_2O) as precursors perform deposition with reactants at pressures of 0.3 mbar and 0.8 mbar, with pulse times of 0.1 sec and 0.05 sec, respectively.[27]
    2. Following each gas pulse, purge the reactor with Ar for 60 sec at 0.2 mbar to ensure minimal background deposition due to physisorbed reactants. For the masks in this work, 80 ALD cycles are used to grow approximately 2.8 nm of amorphous titania at 100 °C.

4. Slowly vent ALD chamber with Ar gas and open. Repeat steps 4.1 and 4.2 for sample transport.

6. Atomic Force Microscopy (AFM)

1. Ensure proper calibration of the AFM according to manufacturer's protocol. Open sample transporter and gently remove sample using tweezers.
2. After removing from transporter, securely install the sample into the AFM using a mechanical mounting method such as a clamping system if possible. Focus the AFM camera onto the sample, and locate the fiducial markings on the sample surface to align the AFM tip to the pattern based on the optical metrology in step 3.2.
3. Ensure that the AFM settings will show both the height and phase information and set the scan size to be between 20 and 40 μm wide. Engage the AFM tip onto the sample.
4. Using the height and phase information at highest resolution, scan until the locator patterns region are identified. Zoom into the patterned region and locate the region in which an image is desired.
5. Take an image of the desired regions using the appropriate image quality and resolution (typically the highest possible). Once all desired regions have been scanned, disengage the tip from the sample. Unload the sample. Repeat steps 4.1 and 4.2 for sample transport.

7. Reactive Ion Etching

1. Chill capacitively coupled RIE reactor to -110 °C, then load the sample into its intro chamber and pump down to 7.5×10^{-6} mbar.
    1. Stabilize the temperature for 3 min. Then turn the gas on with flow rates of O_2 at 8 sccm (standard cubic centimeter per minute), Ar at 40 sccm, and SF_6 at 20 sccm.
    2. Strike plasma using a 150 W RF discharge, then modify the gas flow to etch for 1 min using SF_6 at 52 sccm and O_2 at 8 sccm. Interaction of these gases with Si will etch at a rate of approximately 20 nm/min.[30]
    3. Pump vacuum to 7.5×10^{-6} mbar. Vent RIE system. Repeat steps 4.1 and 4.2 for sample transport.

8. Scanning Electron Microscopy (SEM)

1. SEM Sample Mounting and introduction of sample to system.
    1. Place non-adhesive sample mount into a convenient location to facilitate sample mounting.

2. Open sample transporter and gently remove sample using tweezers to grab the sample by the edges and securely install into SEM mount, then introduce sample assembly into SEM.
3. Vent and open SEM chamber. Securely install sample assembly to the SEM sample stage. Pump down SEM chamber.

2. Locate the fiducials.
   1. Bring the magnification to lowest possible value. Select the accelerating voltage and beam current settings that would give good resolution. Start with lowest acceptable settings. Go up as needed.
   2. Turn on the electron beam. Bring the general region of interest to recommended working distance and eucentric height.
   3. Locate and focus on fiducials described in section 1.1. Adjust working distance as necessary. Optimize the focus, brightness and contrast.

3. Locate and image the patterns.
   1. Relative to the fiducials, locate the patterns based on the optical metrology of section 3.2 and AFM metrology of section 6. To minimize carbon deposition on patterns, optimize focus using nearby non-essential features. Once optimized, move to the patterns and acquire plan view images and measurements.
   2. If needed, tilt the sample for 3D images and pattern height measurements. For other patterns, repeat from 8.3 as needed.

4. Perform SEM system closing routine and dismount sample/s, as prescribed by the SEM manufacturer. Secure the sample back into the transporter.
5. Repeat steps 4.3 and 4.4 for sample transport and storage. At this point, the samples are robust and can be stored for an indefinite period of time. Perform post-imaging analyses if necessary.

Representative Results

In the cases described here, HDL is performed using multi-mode lithography.[24] In FE mode, performed with 8 V sample bias, 1 nA, and 0.2 mC/cm (equivalent to 50 nm/sec tip speed), the tip moves over the surface either parallel or perpendicular to the Si lattice, producing lines of depassivation. While this lineshape is very tip dependent, in the case here, the completely depassivated portion of the lines was approximately 6 nm wide, with tails of partial depassivation extending another 2 nm on either side of the line. When highly precise patterns are desired, AP mode lithography is performed using 4 V sample bias, 4 nA, and 4 mC/cm (equivalent to 10 nm/sec tip speed). The extent of the AP mode component of each pattern depends upon the width of the partially depassivated patterns produced using FE mode. See **Figure 2** for examples of STM images of patterns on Si(100)-H for the various HDL modes. **Figure 2A** shows a small pattern produced using only AP mode HDL. **Figure 2B** is an example of a pattern written using multi-mode lithography, where the FE mode lines were approximately 6 nm wide, but were written on an 10 nm pitch, with approximately 2 nm of each edge written using AP mode HDL. The FE mode portions in the interior of the pattern were written on a pitch of 10 nm, so there are narrow regions within the pattern where HDL was incomplete. For large, imprecise patterns FE mode can be used alone, as in **Figure 2C** where an approximately 1 μm^2 *serp* pattern was written on a 20 nm pitch.

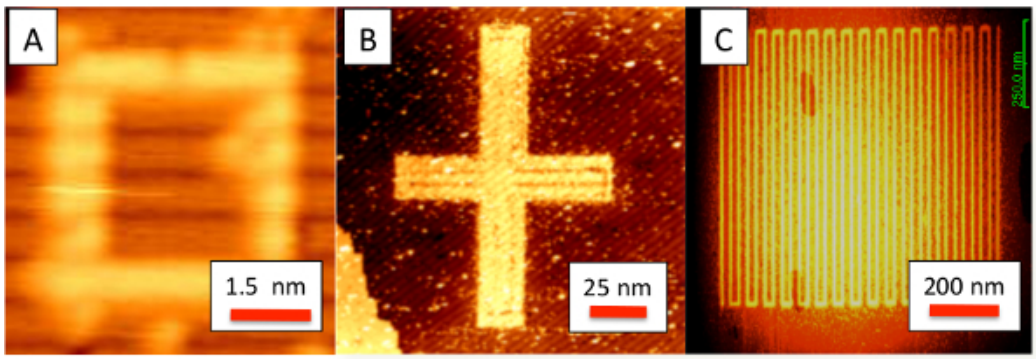

Figure 2. Representative HDL patterns. (**A**) STM image of an HDL pattern written with AP mode lithography of 4V, 4 nA, and 4 mC/cm (10 nm/sec). (**B**) STM image of a multi-mode HDL pattern written using a combination of AP mode and FE mode (8V, 1 nA, 0.2 mC/cm). The FE mode line pitch was chosen to be slightly larger than the written linewidth to improve the visibility of the vectors used in writing. (**C**) FE mode lithography of a large locator *serp* written on a 20 nm pitch. Please click here to view a larger version of this figure.

In order to achieve the best mask production using atomically precise HDL patterns, a high degree of selectivity must be possible. Previously, the ALD selectivity has been investigated by XPS and other methods comparing deposition on unpatterned Si(100)-H and Si(100)-SiO_x surfaces as an analogs for the unpatterned and patterned areas, respectively.[27,31] Using atomic force microscopy (AFM), we observe similar results, as shown in **Figure 3**. 200 nm x 200 nm squares were patterned onto Si(100)-H with >90% of the hydrogen removed within the patterns, and then titania was deposited on the patterns. AFM analysis of the patterns compared to the background showed that there was a taller layer of growth on-pattern than the height of tallest defect on the background. Extrapolation of the growth curves for the on-pattern and background deposition indicate an identical growth rate, but with an incubation of 20 cycles for the tallest background growth. It is worth reiterating here that most of the background growth occurs with a much longer incubation time. As described above, the Ar purge step is of great importance in order to achieve selectivity because it helps remove physisorbed precursors. Preliminary results with other titania precursors, such as tetrakis(dimethylamino)titanium, show more background reactivity, presumably because the precursors physisorb too strongly to the Si(100)-H surface. To prevent background adsorption, careful attention to the precursor chemistry is of great importance.

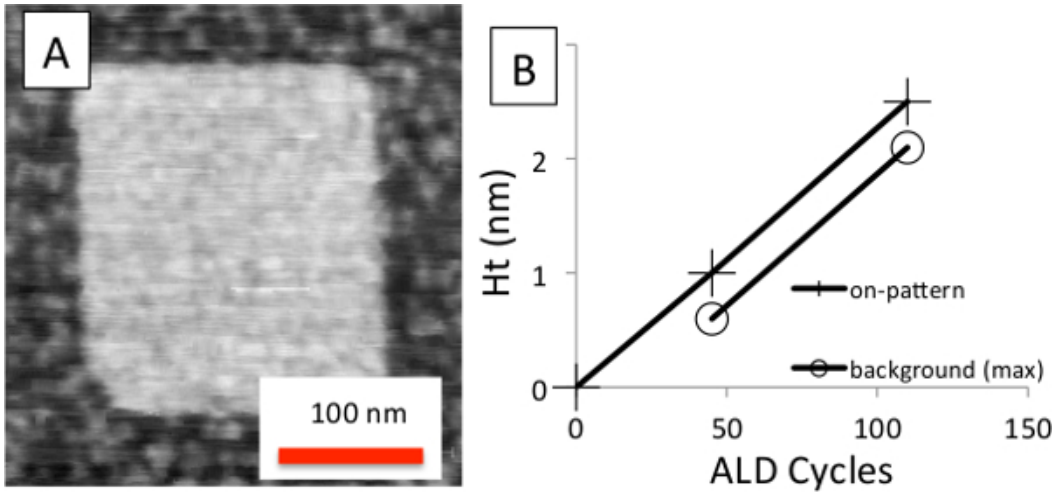

Figure 3. Selectivity of deposition. (**A**) Sample AFM image showing TiO_2 deposition on patterned and background areas. Deposition was carried out at 100 °C. (**B**) Deposition depths for various numbers of cycles. The crosses represent the height as measured by AFM of the growth "on pattern" relative to the background. The open circles show the height as measured by AFM of the *tallest* background deposition within an area of 200 nm x 200 nm near a patterned area. Please click here to view a larger version of this figure.

Given that it is possible to deposit onto HDL patterns, investigation of the limits of pattern features should be examined. While it has already been shown that the ALD produces broadened patterns relative to the HDL patterns, and that the etched structures are slightly shrunk relative to the masks, the effect of producing highly dense arrays still remains somewhat unresolved. **Figure 4** shows the HDL, titania mask, and etched structures for an array of squares fabricated using FE mode HDL lines written at a pitch of 15 nm. In **Figure 4A**, the HDL pattern shows two *serps*—one rotated by 90 degrees relative to the other—written with an 8 V tip-sample bias, 1 nA current, and 0.2 mC/cm dose (or 50 nm/sec tip speed). There are clearly openings in the pattern of varying sizes. Within the openings themselves, some HDL has occurred, but it remains low—on the order of 20% H removal. **Figure 4B** shows an AFM image of the same pattern after mask deposition. Due to tip convolution effects, the openings in the pattern are difficult to resolve. However, a clear order is observable. **Figure 4C** is an SEM image of the same pattern after RIE. Approximately 60% of the desired openings were indeed transferred into the substrate, indicating that this pattern size and density is approximately the limit for effective nanostructure fabrication using FE mode HDL.

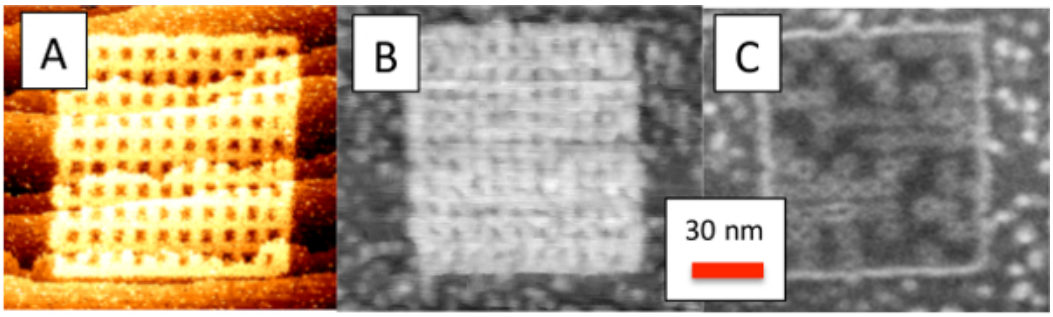

Figure 4. Array of openings. (**A**) STM of HDL with lines written using FE mode. Two serpentine patterns, rotated at 90 degrees relative to each other, are written with a pitch of 10 nm. (**B**) AFM image after 2.8 nm of ALD of TiO_2 of the same pattern. (**C**) SEM of "hole" array after RIE to remove 20 nm of Si. Notice that some "holes" have failed to etch. Please click here to view a larger version of this figure.

Discussion

Performing metrology on the nanostructures described above requires the ability to bridge the tip positioning during HDL and pattern location using other tools such as AFM and SEM. In contrast to other well-developed patterning tools with high-resolution position encoding such as e-beam lithography, the HDL performed here was performed with an STM without well controlled coarse positioning, so extra position identification protocols were used, as shown in **Figure 3**. First, a long-focal-length microscope is positioned outside the UHV system approximately 20 cm from the tip-sample junction. The sample is patterned with a square grid of 10 μm wide lines, 1 μm deep, on a pitch of 500 μm to facilitate identification of the tip location on the surface.

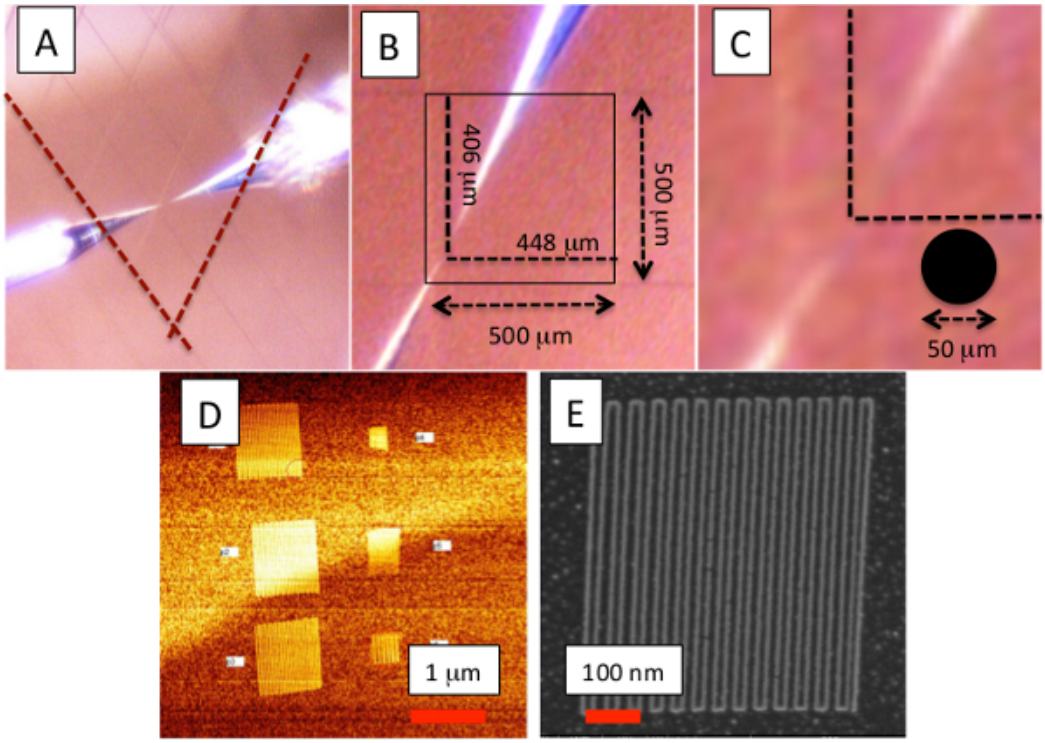

Figure 5. Pattern location images of sample. (**A**) Optical image of STM tip (left) and its reflection (right) in the Si(100) surface on an area of the sample with 500 µm pitch line pattern. The lines are 1 µm deep and 10 µm wide prior to UHV processing. Guide lines are included to show the line directions. (**B**) Close-up, de-skewed optical image of the tip (lower left) and its reflection (upper right). The centerpoint location between the tip and its reflection is identified within the 500 µm x 500 µm fiducial square. **C**: Closeup of patterning location with a 50 µm spot included for scale. **D**: 5 µm x 5 µm AFM image of an entire patterned area after ALD. **E**: 1 µm x 1 µm SEM image of one of the locator patterns after RIE. Please click here to view a larger version of this figure.

The first step to locating nanostructures is identifying the tip location on the surface,[32,33] which is accomplished in this case using a long working distance microscope. **Figure 5A** shows an optical image of the tip when engaged with the sample, with dotted lines added to guide the reader for the directions of the fiducial grid. To locate the tip/sample junction the optical image is unskewed to make a square grid, as shown in **Figure 5B**, although there are errors in high temperature processing of the samples due to significant surface atom migration. This reduces the depth and visibility of the fiducial grid as imaged here, increasing the uncertainty in the tip position.[32] While it has been shown previously that high temperature sample processing will induce significant atomic scale surface reconstruction, the grid pitch used here is great enough to have little effect on the surface reconstruction in the middle of the squared defined by the grid.[34] However, near the edges of the patterned areas, step bunching does occur with asymmetry that depends upon the direction of current flow during sample preparation. [34] Since the optical imaging is performed at an oblique angle relative to the surface, small changes in height on one side of a trench relative to the other will induce additional uncertainty in pattern location—especially when compared to plan-view imaging as in AFM or normal SEM. After the tip engages the sample, the 10 µm focal spot size of the microscope coupled with the ~20 µm post-processing fiducial linewidth results in an approximate uncertainty in pattern position identification of ±27 µm. This defines the search window for using various techniques for pattern identification.

To facilitate the location of the smaller 10–100 nm features, additional large *serps* are added near the nanoscale patterns, as shown in **Figure 5B**. These 800 nm x 800 nm *serps* are written using FE mode HDL with vertical lines and gaps of 15 nm each. By aligning the AFM fast scan direction to be perpendicular to the *serp* lines (*i.e.,* horizontal scanning), these patterns tend to show a high contrast in the AFM phase image due to the high spatial frequency of the topography, further facilitating pattern location. Once these patterns are found, it becomes much easier to find the smaller nanoscale patterns which are placed with approximately 100 nm accuracy relative to the large patterns.

For this nanostructure fabrication process, the sample undergoes atmospheric exposure between each major process step once HDL has been performed, as shown schematically in **Figure 1**. Given this, it must be assured that the sample does not degrade at any point in the handling. As shown above, there is a finite amount of background deposition during ALD, which is assumed to seed on background defect sites.[31] Thus, improper handling such as extended atmosphere exposure can increase the number of background defects and reduce the apparent ALD selectivity. An additional surface degradation mechanism can occur during venting of the sample from the UHV load-lock to atmospheric conditions.[29] To alleviate this problem, a spring-loaded sapphire chip which was mounted onto a linear actuator in UHV makes contact to the 125 µm thick sample mounting foil which contacts the sample to prevent surface degradation. Once the sample is at atmospheric conditions, the rate of dangling bond accumulation remains low (*i.e.,* <0.1%/hr) for at least several hours, so as long as the sample is inserted into a stable environment such as ultra-pure Ar within less than 1 hr, the additional background deposition due to surface damage should remain low. At this point, it should be noted that the sample should not be stored in a vacuum environment, as this requires an additional vent/pump-down cycle, adding to the possibility of surface damage. This time between HDL and ALD is the point at which the sample is most sensitive since the etch mask has not yet been applied. After ALD, the sample still needs protection, but only to prevent additional mask growth due to silicon dioxide formation, a comparatively slow process.

In the patterns shown in **Figure 4**, the HDL removed >80% of the background H within the center of the patterns, with a spatial roll-off in the efficiency of the depassivation as the edge of the line is reached.[24] Given the limits of very limited ALD on the background and incubation free growth on fully depassivated patterns (**Figure 3**), the edges of FE mode patterns where there is a transition from fully effective HDL and no HDL, show a transition of effectiveness of ALD mask growth. Below 70% H removal during HDL is where this transition starts to occur, indicating an approximate region of ~2 nm on each side of an FE mode line where partial mask deposition occurs.[35] Additionally, ALD growth occurs in a "mushroom" manner,[36] further broadening the mask relative to the HDL patterns so that a mask of 2.8 nm broadens any mask features by that amount. To summarize, the ALD linewidth can be expressed as $W_m = W_{sat} + f(\delta H) + M$ where W_m is the total width, W_{sat} is the width of the line where the HDL has saturated to remove >70% of the surface H, $f(\delta H)$ is the additional width due to the growth at each point due to the density of H remaining on the surface, and M is the additional linewidth due to the mushrooming of growth. δH depends upon the spatial distance from the saturated edge of the HDL pattern, so $f(\delta H)$ becomes $f(r)$ since there is spatial dependence of the HDL. Of these terms, W_{sat} plays the primary role in the overall linewidth, and the other terms determine the degree of roll-off of the line edges.

With the ultimate nanostructure fabrication, the ALD mask alone does not determine the total feature size. Instead, the pattern size depends upon the degree of erosion of the substrate under the mask. The total etched linewidth is expressed as $W_t = W_m - W_e = W_{sat} + f(r) + M - W_e$, where W_e indicates an erosion linewidth, or pattern size reduction due to the etching process. This depends upon, among other things, the thickness and quality of the etch mask as described above for W_m. For a case where the linewidth simply requires the removal of mask before etching occurs, the W_e term is zero, however it is observed that there is a modification to the feature size after etching relative to the mask shape, suggesting that more complicated dynamics are at play.

Of the elements determining linewidth limitations, W_{sat} can be reduced to a minimum width of ~4 nm before the growth stops appearing the same as bulk ALD.[35] Of the other elements the mushroom growth effect, M (and as a consequence W_m), can only be reduced if the total film thickness is reduced, correlating with the total nanostructure height after etching. The line broadening effect due to the spatial dependence of the density of H remaining on the surface, $f(\delta H)$, can be reduced to nearly zero by using multi-mode HDL which produces HDL line edges with negligible line edge roll-off.[24] To demonstrate the effect of this reduction in $f(\delta H)$, **Figure 6** shows a pattern array of squares produced using multi-mode HDL. The array includes patterns with HDL linewidths of 7 nm, 14 nm, and 21 nm from top to bottom, and inner HDL opening sizes of 7 nm, 14 nm, and 21 nm from left to right. While there is a slight misalignment of the multi-mode HDL in the bottom row, along the top row the registration is precise to <1 nm. After RIE, the lines remain primarily intact to widths of 5 nm with two small defects, and the openings between lines are resolvable for all of the patterns with the 7 nm holes barely resolvable using this metrology tool.

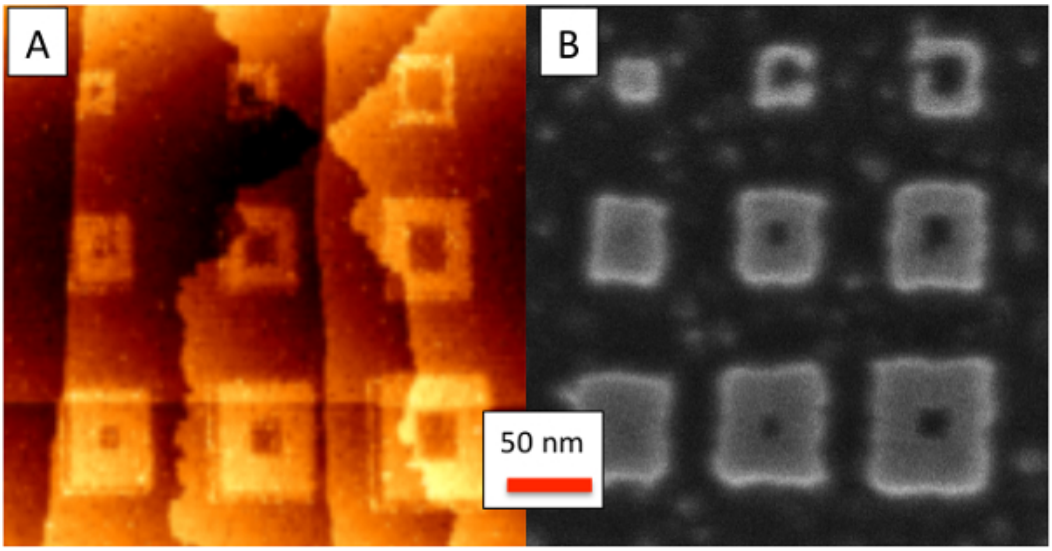

Figure 6. Linewidth and holewidth test. (**A**) STM of HDL of boxes written using multi-mode HDL. The linewidth of rows is 21 nm, 14 nm, and 7 nm from the bottom to the top, respectively, and the holewidth of the columns is 7 nm, 14 nm, and 21 nm from left to right, respectively. (**B**) SEM of the same patterns after ALD and RIE. Please click here to view a larger version of this figure.

The ultimate limits of this process depend upon selectivity of the ALD process, the quality of the HDL, the resistance of the mask to etching, and the desired feature shapes themselves. Methods to improve selectivity based on chemistry and background defect mitigation has already been addressed above. It has been shown previously that leaving H defects in the patterned areas reduces the quality of mask growth, and thus the resistance to etching.[35] Also, lack of careful control over the patterned line edges results in a mask "roll-off", or excessive thinning of the mask along the edges of patterns which acts as a proximity effect preventing close placement of patterns. Fortunately, the selectivity of the etch process depends upon the mask thickness, so for spurious deposition on the background or defects along the edges of patterns the net effect is small. Furthermore, for structures shorter than 20 nm, thinner mask layers will likely be possible. Since the ALD growth occurs in a mushroom manner, thinner masks due to shorter structures will result in even better lateral control and smaller features than those demonstrated here. While the ultimate feature size reductions are not known for this process, certainly some down-scaling is likely.

While the SEM metrology leaves uncertainty regarding feature size and positioning, the first metrology step described in the top of **Figure 1** gives atomic precision with regard to the HDL pattern as written. Since the Si(100)-H surface consists of a very regular lattice, and since the STM can be operated in a non-destructive imaging mode, the HDL patterns can be imaged without inducing further surface damage or further patterning, in contrast to other techniques such as e-beam lithography. With the atomic scale imaging of the invariant Si(100) lattice, the STM metrology eliminates the largest part of the positioning uncertainty related to the AFM and SEM metrology steps. In **Figure 6B** the box array appears skewed, for example. With the high resolution metrology of the STM giving atomic precision of the feature positions within the array, the

apparent skew can be confirmed to be due to SEM imaging artifacts. Also, with highly precisely known spacings between the array features, an additional calibration uncertainty with respect to linewidths in the SEM images is eliminated.

This manuscript describes a nanofabrication method which utilizes the atomic precision of scanning tunneling microscope-based hydrogen depassivation lithography (HDL). HDL produces chemically reactive patterns on a Si(100)-H surface where atomic layer deposition of titania produces a localized etch mask with a lateral dimension demonstrated down to below 10 nm. Reactive ion etching then transfers the HDL patterns into the substrate, making 17 nm tall patterns with high precision lateral control. In order to achieve these results, samples must be protected during venting and transfer between instruments. With careful control of sample handling, nanostructures with traceability to the atomic lattice can be fabricated with atomic position precision and ~1 nm size precision.

Disclosures

The authors have nothing to disclose.

Acknowledgements

This work was supported by a Contract from DARPA (N66001-08-C-2040) and by a grant from the Emerging Technology Fund of the State of Texas. The authors would like to acknowledge Jiyoung Kim, Greg Mordi, Angela Azcatl, and Tom Scharf for their contributions related to selective atomic layer deposition, as well as Wallace Martin and Gordon Pollock for *ex-situ* sample processing.

References

1. Yoffe, A. D. Low-dimensional systems: quantum size effects and electronic properties of semiconductor microcrystallites (zero-dimensional systems) and some quasi-two-dimensional systems. *Adv. in Phy..* **42** (2), 173–262, doi: 10.1080/00018739300101484 (1993).
2. Alivisatos, A. P. Semiconductor Clusters, Nanocrystals, and Quantum Dots. *Science* . **271**, (5251), 933–937, doi: 10.1126/science.271.5251.933 (1996).
3. Craighead, H. G. Nanoelectromechanical Systems. *Science.* **290**, (5496), 1532–1535, doi: 10.1126/science.290.5496.1532 (2000).
4. Dai, M. D., Kim, C.-W., & Eom, K. Finite size effect on nanomechanical mass detection: the role of surface elasticity. *Nanotechnology.* **22** (26), 265502, doi: 10.1088/0957-4484/22/26/265502 (2011).
5. Personick, M., & Mirkin, C. Making sense of the mayhem behind shape control in the synthesis of gold nanoparticles. *J. Am. Chem. Soc..* **135** (C), 18238–18247, doi:10.1021/ja408645b (2013).
6. Rothemund, P. W. K., Ekani-Nkodo, A., *et al*, Design and Characterization of Programmable DNA Nanotubes. *J. Am. Chem. Soc..* **26**, 16344-16353, doi: 10.1021/ja044319l (2004).
7. Hersam, M. C., Guisinger, N. P., & Lyding, J. W. Silicon-based molecular nanotechnology. *Nanotechnology.* **11** (2), 70–76, doi: 10.1088/0957-4484/11/2/306 (2000).
8. Eigler, D. M., & Schweizer, E. K. Positioning single atoms with a scanning tunnelling microscope. *Nature.* **344**, 524–526, doi: 10.1038/344524a0 (1990).
9. Heinrich, A. J., Lutz, C. P., Gupta, J. A., & Eigler, D. M. Molecular cascades. *Science.* **298**, 1381–1387, doi: 10.1126/science.1076768 (2002).
10. Crommie, M. F., Lutz, C. P., Eigler, D. M. Confinement of Electrons to Quantum Corrals on a Metal Surface. *Science.* **262** (5131), 218–220, doi: 10.1126/science.262.5131.218 (1993).
11. Shen, T.-C., Wang, C., *et al..* Atomic-Scale Desorption Through Electronic and Vibrational Excitation Mechanisms. *Science.* **268** 1590–1592, doi: 10.1126/science.268.5217.1590 (1995).
12. Randall, J. N., Lyding, J. W., *et al..* Atomic precision lithography on Si. *J. Vac. Sci. Tech. B.* **27** (6), 2764–2768, doi: 10.1116/1.3237096 (2009).
13. Tong, X., & Wolkow, R. A. Electron-induced H atom desorption patterns created with a scanning tunneling microscope: Implications for controlled atomic-scale patterning on H-Si(100). *Surf. Sci..* **600** (16), L199 – L203, doi: 10.1016/j.susc.2006.06.038 (2006).
14. Hitosugi, T., Hashizume, T., *et al..* Scanning Tunneling Spectroscopy of Dangling-Bond Wires Fabricated on the Si(100)-2x1-H Surface. *Jap. J. App. Phys, Pt 2 2.* **36** (3B), L361–L364, doi: 10.1143/JJAP.36.L361 (1997).
15. Bird, C. F., Fisher, A. J., & Bowler, D. R. Soliton effects in dangling-bond wires on Si(001). *Phys. Rev B.* **68** 115318, doi: 10.1103/PhysRevB.68.115318 (2003).
16. Wolkow, R. A., & Livadaru, L., *et al..* Beyond-CMOS Electronics. 1–28 at <http://arxiv.org/abs/1310.4148>, (2013).
17. Lyding, J. W., Shen, T.-C., Hubacek, J. S., Tucker, J. R., & Abeln, G. C. Nanoscale patterning and oxidation of H-passivated Si(100)-2×1 surfaces with an ultrahigh vacuum scanning tunneling microscope. *App. Phys. Lett..* **64** (15), 2010–2012, doi: 10.1063/1.111722 (1994).
18. Lyding, J. W., Shen, T.-C., Abeln, G. C., Wang, C., & Tucker, J. R. Nanoscale patterning and selective chemistry of silicon surfaces by ultrahigh-vacuum scanning tunneling microscopy. *Nanotechnology.* **7** 128–133, doi: 10.1088/0957-4484/7/2/006 (1996).
19. Owen, J. H. G., Ballard, J., Randall, J. N., Alexander, J., & Von Ehr, J. R. Patterned Atomic Layer Epitaxy of Si / Si(001):H. *J. Vac. Sci. Tech. B.* **29** (6), 06F201, doi: 10.1116/1.3628673 (2011).
20. Goh, K. E. J., Chen, S., Xu, H., Ballard, J., Randall, J. N., & Ehr, J. R. Von Using patterned H-resist for controlled three-dimensional growth of nanostructures. *App. Phys. Lett..* **98** (16), 163102, doi: 10.1063/1.3582241 (2011).
21. Ye, W., Peña Martin, P. a, *et al..* Direct writing of sub-5 nm hafnium diboride metallic nanostructures. *ACS Nano.* **4** (11), 6818–24, doi: 10.1021/nn1018522 (2010).
22. Brien, J. L., Schofield, S. R., *et al..* Scanning tunnelling microscope fabrication of arrays of phosphorus atom qubits for a silicon quantum computer. *Smart Mat. and Struct.* . **11** (5), 741–748, doi: 10.1088/0964-1726/11/5/318 (2002).
23. Van Oven, J. C., Berwald, F., Berggren, K. K., Kruit, P., Hagen, C. W. Electron-beam-induced deposition of 3-nm-half-pitch patterns on bulk Si. *J. Vac. Sci. Tech. B.* **29** (6), 06F305, doi: 10.1116/1.3640743 (2011).
24. Ballard, J. B., Sisson, T. W., *et al..* Multimode hydrogen depassivation lithography: A method for optimizing atomically precise write times. *J. Vac. Sci. Tech. B.* **31**, (6), 06FC01, doi: 10.1116/1.4823756 (2013).

25. Randall, J. N., Ballard, J. B., *et al.*. Atomic precision patterning on Si: An opportunity for a digitized process. *Microelec. Eng.*. **87** (5-8), 955–958, doi: 10.1016/j.mee.2009.11.143 (2010).
26. Perrine, K. A., & Teplyakov, A. V Reactivity of selectively terminated single crystal silicon surfaces. *Chem. Soc. Rev.*. **39** (8), 3256–3274, doi: 10.1039/B822965C (2010).
27. McDonnell, S., Longo, R. C., *et al.*. Controlling the Atomic Layer Deposition of Titanium Dioxide on Silicon: Dependence on Surface Termination. *The J. Phys. Chem. C.* **117** (39), 20250–20259, doi: 10.1021/jp4060022 (2013).
28. Kane, D. F. Plasma cleaning of metal surfaces. *J. Vac. Sci. Tech.*. **11** (3), 567, doi: 10.1116/1.1318069 (1974).
29. Hersam, M. C., Guisinger, N. P., Lyding, J. W., Thompson, D. S., & Moore, J. S. Atomic-level study of the robustness of the Si(100)-2×1:H surface following exposure to ambient conditions. *App. Phys. Lett.*. **78**,(7), 886–888, doi: 10.1063/1.1348322 (2001).
30. Agostino, R., & Flamm, D. L. Plasma etching of Si and SiO_2 in SF_6–O_2 mixtures. *J. App. Phys.* . **52** (1), 162, doi: 10.1063/1.328468 (1981).
31. Longo, R. C., McDonnell, S., *et al.*. Selectivity of metal oxide atomic layer deposition on hydrogen terminated and oxidized Si(001)-(2×1) surface. *J. Vac. Sci Tech. B.* **32** (3), 03D112, doi: 10.1116/1.4864619 (2014).
32. Ruess, F. J., Oberbeck, L., *et al.*. The use of etched registration markers to make four-terminal electrical contacts to STM-patterned nanostructures. *Nanotechnology.* **16**, (10), 2446–2449, doi:10.1088/0957-4484/16/10/076 (2005).
33. Ruess, F. J., Pok, W., *et al.*. Realization of Atomically Controlled Dopant Devices in Silicon. *Small.* **3**, (4), 563–567, doi: 10.1002/smll.200600680 (2007).
34. Li, K., Namboodiri, P., *et al.*. Controlled formation of atomic step morphology on micropatterned Si (100). *J. Vac. Sci. Tech. B.* **29** (4), 041806, doi: 10.1116/1.3610955 (2011).
35. Ballard, J. B., Owen, J. H. G., *et al.*. Pattern transfer of hydrogen depassivation lithography patterns into silicon with atomically traceable placement and size control. *Journal of Vacuum Science and Technology B.* **32**, (4), 041804, doi: 10.1116/1.4890484 (2014).
36. Gusev, E. P., Cabral Jr., C., Copel, M., D'Emic, C., & Gribelyuk, M. U ltrathin HfO 2 films grown on silicon by atomic layer deposition for advanced gate dielectrics applications. *Microelectronic Engineering.* **69**, 145–151, doi: 10.1103/PhysRevB.68.115318 (2003).

